

https://doi.org/10.1070/QEL16325

Hydrogen generation by laser irradiation of colloids of iron and beryllium in water

I.A. Sukhov, G.A. Shafeev, E.V. Barmina, A.V. Simakin, V.V. Voronov, O.V. Uvarov

Abstract. **The hydrogen generation under irradiation of aqueous colloids of iron and beryllium nanoparticles by 10-ns pulses of the first harmonic of a Nd:YAG laser with an energy density of about 80 J cm^{-2} in the solution is experimentally investigated. The partial hydrogen content in the atmosphere above the colloidal solutions of nanoparticles first increases with increasing irradiation time and then reaches a stationary level (400–500 Torr). The hydrogen generation rate, being nonzero in the case of irradiation of pure water, passes through a maximum with an increase in the nanoparticle concentration. The results obtained are discussed in terms of the dissociation of water molecules under a direct electron impact from the optical breakdown plasma formed in the liquid.**

Keywords: *hydrogen generation, laser irradiation, colloids of iron and beryllium.*

1. Introduction

Laser ablation of solids in liquids is a physical method of fabricating various nanoparticles. If the laser beam energy density on the target placed in a liquid is sufficiently high for melting the target surface, the molten region is sputtered in the form of nanoparticles under the recoil pressure of the liquid vapour. Many metals used as targets (e.g., gold or silver) have a high melting temperature (on the order of 10^3 K). At this temperature, the liquid vapour contacting with the molten region may undergo chemical changes. This effect is indeed observed, for example, during laser ablation of a brass or bronze target in ethanol [1]. The generation of nanoparticles of the corresponding alloys is accompanied by ethanol pyrolysis up to the formation of glassy carbon, as evidenced by the Raman spectra of dry nanoparticles. One might expect the formation of other reaction products (in particular, gaseous) during laser ablation of solids in liquids.

The generation of nanoparticles during laser ablation in liquids occurs under nonequilibrium conditions, characterised by large temperature and pressure gradients. Therefore, we can suggest that the chemical decomposition of the liquid surrounding the target may occur in a different way as compared with isothermal heating. In addition, the elevated temperature in the laser-irradiated region may facilitate the catalytic effect of the newly formed nanoparticles on the liquid vapour. The generation of nanoparticles of noble metals (Au, Ag) has been investigated in many studies. In particular, the formation of nanoparticles of these metals in water is accompanied by the generation of gaseous hydrogen [2]. Laser irradiation of colloidal solutions gives rise to the so-called nanoplasma around the nanoparticles located in the laser beam waist [3]. At sufficiently high nanoparticle concentrations, these plasma particles may merge into a microscopic plasma of the laser breakdown in the liquid. It is of interest to study this process when fabricating nanoparticles of other metals (with a higher reactivity).

In this study, we chose iron and beryllium as target metals. Iron nanoparticles have already been successfully obtained by laser ablation in organic liquids (ethanol, isopropyl alcohol) and in water [4, 5]. An analysis of their transmission electron microscope (TEM) images shows that the particles have a contrast core, presumably consisting of metallic iron, and a less contrast iron oxide shell. The existence of metallic iron lattice is confirmed by X-ray diffraction patterns of the nanoparticle powder. It should be noted that particles with a metal core can be formed even in experiments on laser ablation of iron in water [5], despite the high temperature and large specific surface of the metal sputtered into water. This fact indicates low reactivity of shell vapour, which may be caused by hydrogen generation. In principle, H_2 may suppress oxidation of iron nanoparticles heated to a high temperature during a laser pulse.

It was shown in our previous work [6] that the beryllium particles obtained by ablation in water are single-crystal ones. An analysis of the optical properties of these nanoparticles showed that their colloidal solution is transparent for visible light and absorbs only in the far-UV spectral region. Thus, the interaction of beryllium nanoparticles with radiation in the visible and IR ranges is weaker than that of iron nanoparticles; however, beryllium nanoparticles may also have a metal core. Therefore, it is of interest to compare the hydrogen generation efficiency under irradiation of beryllium and iron nanoparticles.

I.A. Sukhov Wave Research Center, A.M. Prokhorov General Physics Institute, Russian Academy of Sciences, ul. Vavilova 38, 119991 Moscow, Russia; Moscow Institute of Physics and Technology, Institutskii per. 9, 141700 Dolgoprudnyi, Moscow region, Russia; e-mail: sukhov@phystech.edu;
G.A. Shafeev Wave Research Center, A.M. Prokhorov General Physics Institute, Russian Academy of Sciences, ul. Vavilova 38, 119991 Moscow, Russia; National Research Nuclear University 'MEPhI', Kashirskoe sh. 31, 115409 Moscow, Russia; e-mail: shafeev@kapella.gpi.ru;
E.V. Barmina, A.V. Simakin, V.V. Voronov, O.V. Uvarov Wave Research Center, A.M. Prokhorov General Physics Institute, Russian Academy of Sciences, ul. Vavilova 38, 119991 Moscow, Russia

Received 20 February 2017; revision received 5 April 2017
Kvantovaya Elektronika **47** (6) 533–538 (2017)
Translated by Yu.P. Sin'kov

2. Experimental

Beryllium and iron particles were formed by laser ablation of bulk targets in a liquid. The beam of an ytterbium-doped fibre laser with a wavelength of 1060–1070 nm was focused using an objective (f = 42 cm) onto the surface of a metal plate immersed in water having a volume of 4 mL. The thickness of the liquid layer above the target did not exceed 1 mm. The laser pulse duration was 8 ns, the pulse repetition rate was 200 kHz, and the pulse energy was 0.1 mJ. The focused beam was moved over the sample surface with a velocity of 300 mm s^{-1} using a system of mobile mirrors with an electric drive. To minimise the repeated effect of laser radiation on the particles formed, the exposure time was chosen to be no longer than 2 min [7]. The size distributions of the particle mass and number of particles were measured using a CPS disk centrifuge. The concentrations of beryllium and iron particles in the obtained colloids were, respectively, 13 and 72 μg mL^{-1}.

A powder of beryllium nanoparticles obtained by ablation was also investigated by X-ray diffraction. Samples of different concentrations in Milli-Q water with a conductivity of 0.6 μS were fabricated from the colloids. Then each sample (4 mL in volume) was exposed to 1064-nm Nd:YAG laser pulses; the pulse duration was 10 ns, the pulse repetition rate was 10 kHz, and the pulse energy was 2 mJ. During irradiation the laser beam was moved along a circular trajectory with a velocity of 1000 mm s^{-1} using a system of mobile mirrors with an electric drive (Fig. 1). The laser beam waist was located in the cell with colloid at a distance of 2–3 mm from the input window surface (above it); it formed a plasma ring (visible by the naked eye) during circular motion. Focusing was performed by an objective with a focal length of 90 mm. The laser spot diameter in the focus was about 50 μm.

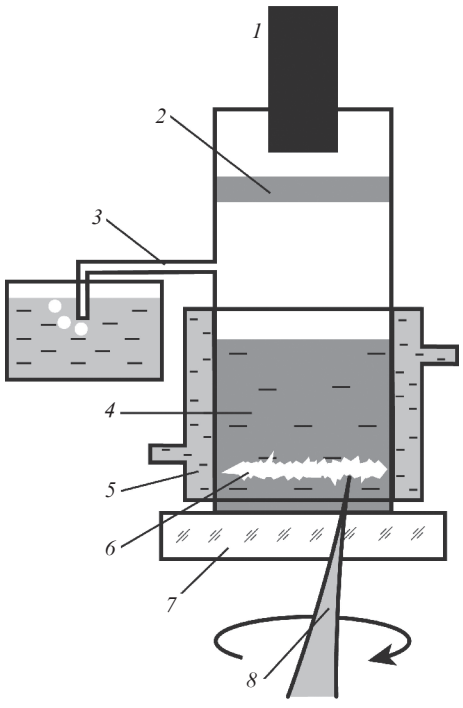

Figure 1. Experimental setup for studying the hydrogen generation: (*1*) electrode; (*2*) membrane; (*3*) capillary; (*4*) colloidal solution; (*5*) cooling system; (*6*) plasma ring; (*7*) window; (*8*) laser beam.

The hydrogen concentration above the colloid surface was measured using an amperometric sensor, which was hermetically mounted in the cell with a sample. The excess pressure caused by the gas formation was relieved using a glass capillary immersed in water to a depth of 1 cm. Thus, the pressure in the cell was equal to atmospheric. The internal electrolyte of the sensor was separated from the volume with the measured gas by a membrane permeable to only hydrogen. The sensor recorded either the hydrogen concentration (in mg L^{-1}) or its partial pressure (in Torr). The sensor was calibrated in air (in the absence of hydrogen) and at a hydrogen pressure of 1 atm. The instrumental measurement error was 5%. The total gas volume above the colloid in our experiment was 10 mL, and the sensor response time was 5 min.

3. Results

The average sizes of the beryllium and iron particles obtained by ablation were, respectively, 35 and 20 nm; at the same time, a large fraction of the material was concentrated in particles having sizes of 450 nm (beryllium) and 50 nm (iron) (Fig. 2).

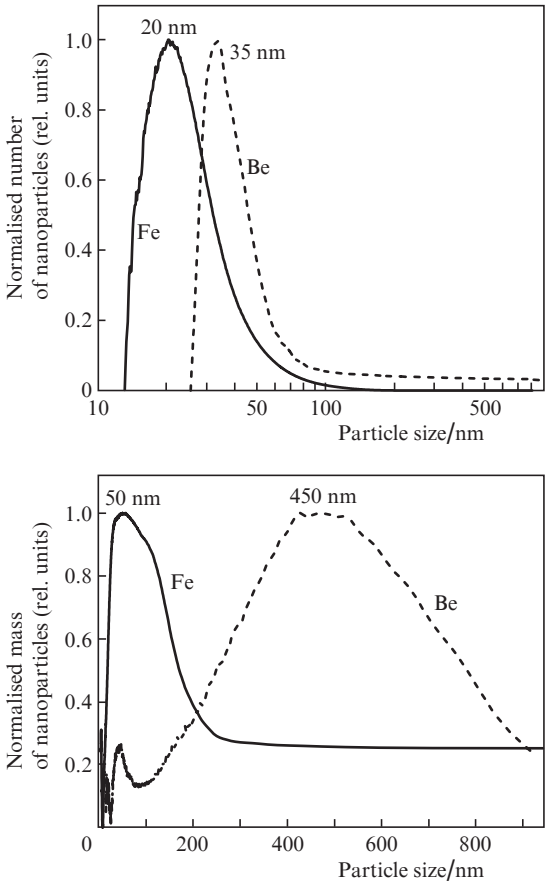

Figure 2. Size distributions of the iron and beryllium nanoparticles used for hydrogen generation.

Images of the nanoparticles obtained by laser ablation of a beryllium target in water are shown in Fig. 3. A high image contrast generally corresponds to the metallic phase of the sample, whereas the regions with a lower contrast can be assigned to beryllium oxide BeO.

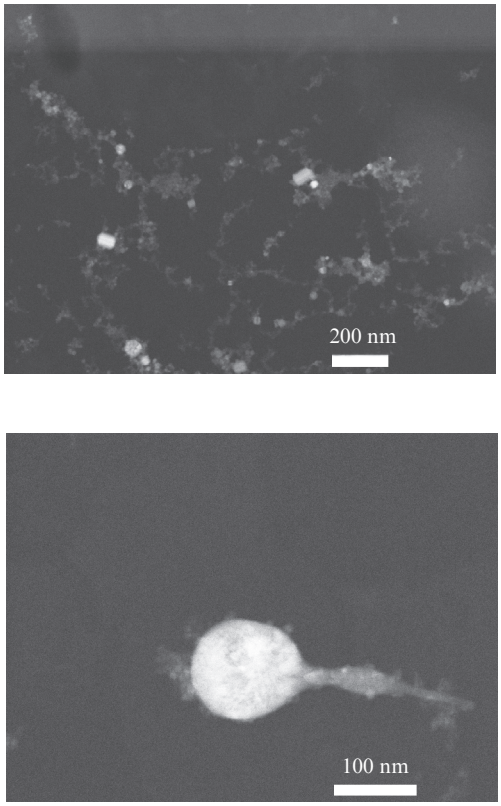

Figure 3. TEM images of (a) beryllium colloid (general view) and (b) high-contrast nanoparticles; the photographs were made in scattered electrons.

The suggestion about the presence of metal nanoparticles in the colloid is confirmed by the diffraction pattern of the dried colloidal solution (Fig. 4). One can see peaks of both metallic Be and BeO. The typical irradiation time of colloids was about 1 h. Since nanoparticles undergo laser fragmentation for this time, their size distribution significantly shifts to smaller values.

The nanoparticles were placed in pure water and then irradiated by a scanning Nd : YAG laser beam. Nanoparticles change their morphology and average size under laser irradiation due to the fragmentation; therefore, the data of Fig. 2 correspond to only the initial particle size. Figure 5 shows dependences of the partial hydrogen pressure in the cell on the irradiation time for samples with different nanoparticle concentrations. It can be seen that the addition of nanoparticles nonmonotonically affects the hydrogen generation: an increase in their concentration first increases the hydrogen yield and then reduces it. However, in both cases, there is an intermediate particle concentration at which the partial hydrogen pressure reaches a maximum. For example, if we compare the partial hydrogen pressures after 20-min irradiation, this concentration for the colloid of beryllium nanoparticles is 0.5 μg mL^{-1}, whereas for iron nanoparticles it amounts to 3 μg mL^{-1} (Fig. 6).

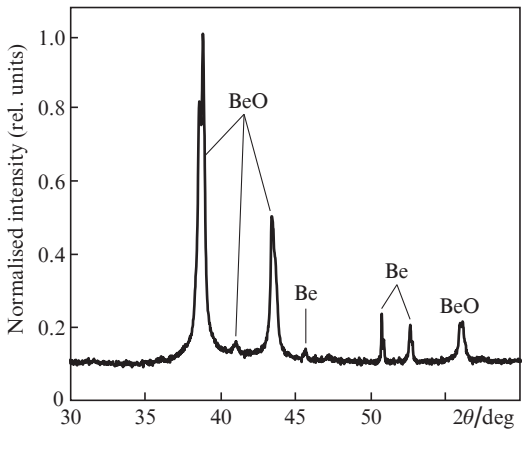

Figure 4. X-ray diffraction pattern of powder of nanoparticles obtained by ablation of a beryllium target in water.

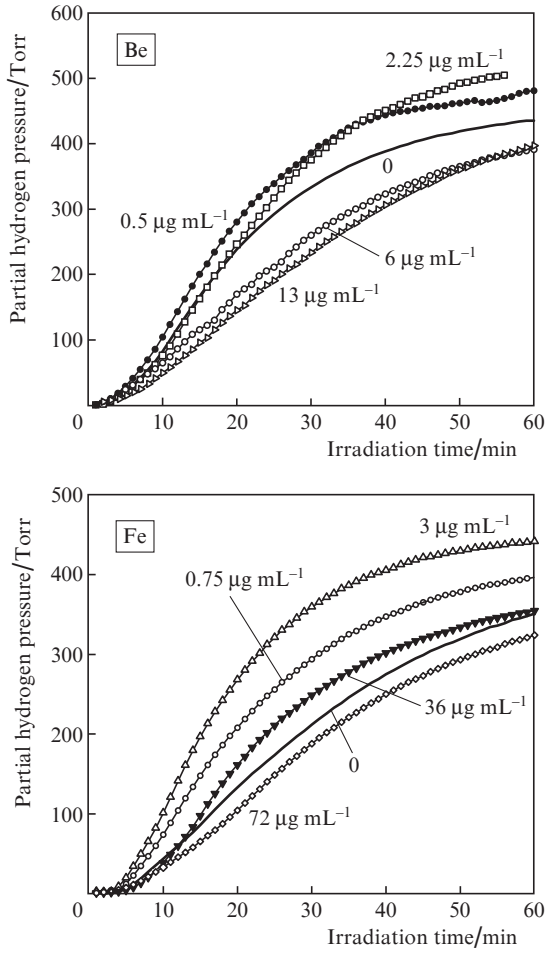

Figure 5. Dependences of the partial hydrogen pressure on the irradiation time of the colloids of beryllium and iron nanoparticles. Colloid concentrations are indicated near curves.

As can be seen in Fig. 5, hydrogen generation is also observed in the case of laser irradiation of pure water (containing no controlled impurities), although introduction of nanoparticles leads to an increase in the partial H_2 pressure.

The maximum hydrogen generation rate is observed at exposure times ranging from 10 to 15 min. A comparison of the absolute values of maximum hydrogen generation rates yields dependences on the colloid concentration (Fig. 7) similar to the concentration dependences of hydrogen pressure.

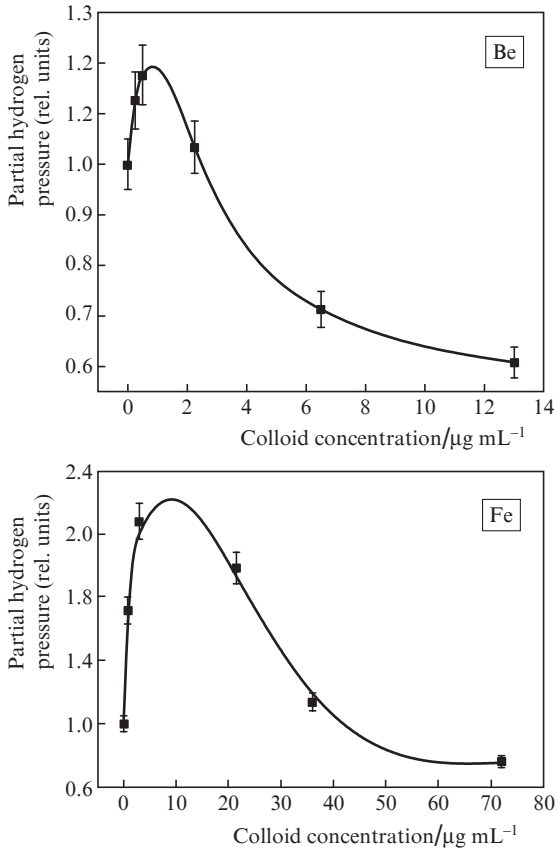

Figure 6. Dependences of the partial hydrogen pressure on the colloid concentration; the exposure time is 20 min; the curves are normalised to the pressure at zero concentration.

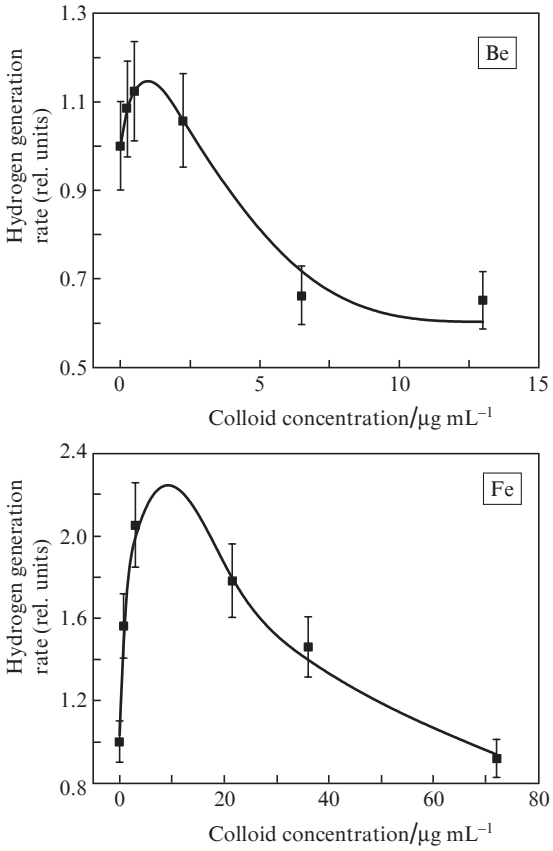

Figure 7. Dependences of the maximum hydrogen generation rate on the nanoparticle concentration; the curves are normalised to the generation rate at zero concentration (pure water).

Figure 7 shows that, in comparison with pure water, the addition of iron nanoparticles affects to a greater extent the hydrogen generation rate than the addition of beryllium nanoparticles. The experiments with different nanoparticle concentrations were performed at identical tunings of the electric drive of the system of mobile mirrors, responsible for the position of laser spot in the cell, because the hydrogen yield depends also on the motion velocity of the beam focused in the cell (Fig. 8).

4. Discussion

The dependences of the partial hydrogen pressure and hydrogen generation rate on the concentration of beryllium and iron nanoparticles have pronounced maxima (Figs 6, 7). Apparently, their existence is due to the dependence of the laser beam intensity in the waist on the particle concentration and on the optical properties of nanoparticles at the laser wavelength. The peak position depends on the nanoparticle material; its variation is explained by the difference in the metal densities (ρ_{Fe} = 7.874 g cm^{-3}, ρ_{Be} = 1.85 g cm^{-3} [8]). Because of this difference, the iron mass exceeds that of beryllium when the numbers of added particles per colloid unit volume are the same. The absorption cross sections of Be and Fe particles of the same size at a wavelength of 1064 nm differ by only 10%, whereas the wavelength-integrated absorption cross section of iron particles is twice as large as the corresponding parameter for beryllium; this ratio is consistent with the difference in the effects of particles on the hydrogen generation rate. The integration over wavelength is justified, because the luminescence spectrum of the liquid breakdown plasma is practically continuous, being determined by the bremsstrahlung of plasma electrons [9]. This result may be due to the formation of a 'nanoplasma' around individual particles [3, 10]. The laser heating of nanoparticles in a dielectric medium (the water used in our experiments can be considered such) was investigated in [10]. Indeed, the laser wavelength (1064 nm) significantly differs from the wavelengths of vibrational and electron levels of H_2O molecules. After form-

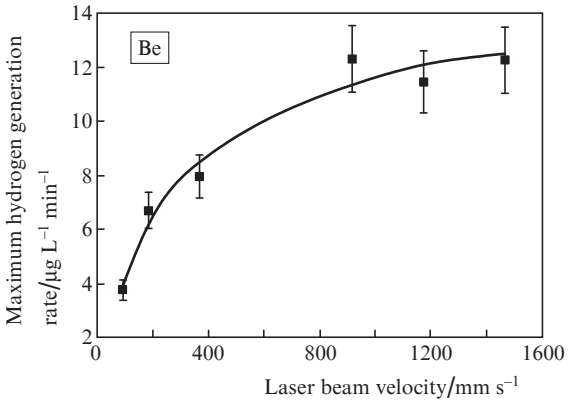

Figure 8. Dependence of the maximum hydrogen generation rate on the laser beam velocity.

ing a nanoplasma, the particles interact not only with the laser radiation but also with the plasma, due to which the particle material significantly affects the absorption cross section. In addition, the nanoplasma formed around individual nanoparticles absorbs laser radiation proportionally to the electron concentration in it. Note that the plasmon resonances of both iron and beryllium nanoparticles in water are also significantly spaced from the laser wavelength (210 nm for Fe nanoparticles with a diameter $d = 10$ nm) [6, 11]. The absorption coefficient k of iron and beryllium at a wavelength of $\lambda = 1064$ nm is 4 [12, 13]; therefore, the absorption of laser radiation by iron nanoparticles with $d \sim \exp(-\alpha d)$ ($\alpha = 2\pi k/\lambda$) is negligible. Hence, the 1064-nm laser radiation is absorbed by only the nanoplasma surrounding individual nanoparticles.

The work function of nanoparticles is smaller than that of bulk material in view of their small radius; therefore, laser radiation induces field electron emission from them [14]. The emitted electrons absorb laser radiation via inverse bremsstrahlung [15], which leads to heating of nanoparticles and causes thermionic emission from them [10]. Laser radiation heats electrons, due to which their average energy increases. When the energy reaches the critical value $E_{cr} \approx 1.5\Delta$ (Δ is the ionisation potential of water molecules (6.5 eV) [16]), water molecules undergo shock dissociation with formation of an electron avalanche. The above-described processes are low sensitive to the nanoparticle morphology, e.g., to the presence of an oxide film on them.

If the concentration of nanoparticles is sufficiently high and the average distance between them is small, individual nanobubbles merge to form a microscopic plasma (the plasma channel length along the laser beam axis was about 100 μm under our experimental conditions). Specifically this circumstance explains the existence of optimal H_2 generation rate with respect to the particle concentration. With a further increase in the concentration of nanoparticles, the scattering of laser radiation from them becomes dominant, and the intensity in the laser beam waist decreases.

The occurrence of microscopic plasma, which can be seen by the naked eye, is accompanied by the formation of large gas bubbles, whose sizes are comparable with the beam diameter. This fact explains the observed dependence of hydrogen generation efficiency on the laser beam velocity (Fig. 8). For example, for a beam velocity of 100 mm s^{-1} and a pulse repetition rate of 10 kHz, the distance between the points exposed to two neighbouring pulses is 10 μm, which is much smaller than the laser spot diameter (50 μm). Therefore, the focusing of the radiation of each subsequent pulse is deteriorated because of the presence of the vapour bubbles formed by the previous pulse. An increase in the beam velocity leads to an increase in the distance between the focusing points of neighbouring pulses. The focusing quality for each subsequent pulse is improved until the distance between the points irradiated by two neighbouring pulses exceeds the gas bubble size. For example, at a velocity of 1000 mm s^{-1}, the exposure points of two neighbouring pulses are spaced by 100 μm, and a further increase in the beam velocity does not affect the hydrogen generation efficiency.

The plasma electrons interact with water molecules, inducing their dissociation. Starting with an electron energy exceeding 16 eV, the dissociation of water molecules caused by the electron impact can be implemented in several different channels. The data reported below were obtained for the interaction between water molecular beams and electron beams of varied energy, with subsequent determination of the composition of reaction products by mass spectroscopy. These channels are as follows [17]:

$$e + H_2O \rightarrow H^+ + OH + 2e \ (E_{ap} = 16.95 \text{ eV});$$

$$e + H_2O \rightarrow H^+ + OH^- + e \ (E_{ap} = 16.00 \text{ eV});$$

$$e + H_2O \rightarrow H^+ + OH(X2P) + 2e \ (E_{ap} = 18.70 \text{ eV});$$

$$e + H_2O \rightarrow H_2^+ + O + 2e \ (E_{ap} = 20.70 \text{ eV});$$

$$e + H_2O \rightarrow HO^+ + H + 2e \ (E_{ap} = 18.11 \text{ eV});$$

$$e + H_2O \rightarrow O^+ + H_2 + 2e \ (E_{ap} = 19.00 \text{ eV});$$

$$e + H_2O \rightarrow O^+ + 2H + 2e \ (E_{ap} = 26.80 \text{ eV}).$$

The subscript 'ap' denotes the instant of appearance of the corresponding products.

The dissociation of water molecules by electron impact from the plasma of liquid breakdown indicates that electrons with necessary energy are present in it at a laser beam intensity of 10^{12} W cm^{-2}, a value used in our experiments. It can also be seen that O and H are present simultaneously in the dissociation products; therefore, the inverse reaction with the formation of H_2O may occur. This circumstance explains the tendency of the partial hydrogen pressure to a constant value during laser irradiation: the newly formed hydrogen reacts again with oxygen to form water. The reaction occurs in the gas bubbles falling in the laser beam and is accompanied by pronounced microexplosions.

One might suggest that the water decomposition product under laser irradiation of the two colloidal nanoparticle solutions under study is also oxygen; preliminary data confirm this suggestion. The hydrogen generation under laser irradiation of carbon powder in water was observed in [18], but at a laser energy density in the medium three orders of magnitude lower than that used by us. It was also reported in [18] about the release of some other gases (CO, CO_2, and CH_4) along with hydrogen. It was suggested in [18] that carbon particles act as a catalyst of the reactions. Apparently, the formation of H_2 under irradiation of carbon powder occurs in the same way as in our study, despite the lower laser energy density in the medium (100 mJ cm^{-2}). This density is sufficient for the formation of 'nanoplasma' on individual particles. Carbon can hardly be considered as a catalyst, because it enters the composition of some reaction products: CO, CO_2, etc.

Hydrogen generation may also occur as a result of laser ablation of bulk targets in water, because scanning the target surface by a laser beam is accompanied by the formation of vapour bubble breakdown plasma, which follows the laser spot on the target. However, this hypothesis needs experimental confirmation.

5. Conclusions

Beryllium and iron nanoparticles were obtained by laser ablation of corresponding metal targets in water using an ytterbium-doped fibre laser with a pulse duration of 8 ns. A beryllium particle consists of a metal core in an oxide shell. The hydrogen generation under irradiation of colloidal solutions

of Be and Fe nanoparticles by a nanosecond neodymium laser with an intensity of $\sim 10^{12}$ W cm^{-2} and a pulse duration of 10 ns was experimentally investigated. It was shown by the example of Be and Fe nanoparticles that the hydrogen yield depends on the particle material, provided that the particles are of the same average size. The optical properties of beryllium and iron differ by only 10% at a laser wavelength of 1064 nm, whereas the ratio of the wavelength-integrated absorption cross sections is consistent with the ratio of hydrogen yields. It was concluded that nanoparticles are additionally heated because they absorb the continuous emission spectrum of the plasma of laser-induced liquid breakdown. The hydrogen generation is related to the formation of optical breakdown plasma on nanoparticles and explained by the dissociation of water molecules under electron impact.

Acknowledgements. This work was supported in part by the Russian Foundation for Basic Research (Grant Nos 15-02-04510_a and 16-02-01054_a) and the RF President's Grants Council (State Support of Young Russian Scientists Programme, Grant No. MK-3606.2017.2).

The authors are grateful to I.V. Baimler for his help in the experiments.

References

1. Sukhov I.A., Shafeev G.A., Voronov V.V., Sygletou M., Stratakis E., Fotakis C. *Appl. Surf. Sci*., **302**, 79 (2014).
2. Barmina E.V., Simakin A.V., Shafeev G.A. *Chem. Phys. Lett*., **655**, 35 (2016).
3. Takeda Y., Kondow T., Mafuné F. *J. Phys. Chem. B*, **110** (5), 2393 (2006).
4. Amendola V., Riello P., Meneghetti M. *J. Phys. Chem. C*, **115**, 5140 (2011).
5. Sukhov I.A., Simakin A.V., Shafeev G.A., Viau G., Garcia C. *Quantum Electron*., **42** (5), 453 (2012) [*Kvantovaya Elektron*., **42** (5), 453 (2012)].
6. Barmina E.V., Sukhov I.A., Lepekhin N.M., Priseko Yu.S., Filippov V.G., Simakin A.V., Shafeev G.A. *Quantum Electron*., **43** (6), 591 (2013) [*Kvantovaya Elektron*., **43** (6), 591 (2013)].
7. Kirichenko N.A., Sukhov I.A., Shafeev G.A., Shcherbina M.E. *Quantum Electron*., **42** (2), 175 (2012) [*Kvantovaya Elektron*., **42** (2), 175 (2012)].
8. Rabinovich V.A., Khavin Z.Ya. *Kratkii khimicheskii spravochnik* (Brief Chemical Handbook) (Leningrad: Khimiya, 1977) pp 57, 62.
9. Serkov A.A., Kuz'min P.G., Rakov I.I., Shafeev G.A. *Quantum Electron*., **46** (8), 713 (2016) [*Kvantovaya Elektron*., **46** (8), 713 (2016)].
10. Grua P., Morreeuw J.P., Bercegol H., Jonusauskas G., Vallee F. *Phys. Rev. B*, **68**, 35424 (2003).
11. Creighton J.A., Eadon D.G. *J. Chem. Soc. Faraday T*, **87** (24), 38811 (1991).
12. Ordal M.A. et al. *Appl. Opt*., **27**, 1203 (1988).
13. Rakić A.D., Djurišic A.B., Elazar J.M., Majewski M.L. *Appl. Opt*., **37**, 5271 (1998).
14. Schertz F. et al. *Phys. Rev. Lett*., **108** (23), 237602 (2012).
15. Ready J.F. *Effects of High Power Laser Radiation* (Orlando: Acad. Press, 1971) p. 261.
16. Williams F., Varama S.P., Hillenius S. *J. Chem. Phys*., **64**, 1549 (1976).
17. Mallard W.G., Linstrom P.J. *NIST Chemistry WebBook, NIST Standard Reference Database Number 69* (Gaithersburg, MD, 2000) p. 20899.
18. Akimoto I., Maeda K., Ozaki N. *J. Phys. Chem. C*, **117** (36), 18281 (2013).